Journal of Alloys and Compounds 838 (2020) 155436

Contents lists available at ScienceDirect

Journal of Alloys and Compounds

journal homepage: http://www.elsevier.com/locate/jalcom

The investigation of electronic, anisotropic elastic and lattice dynamical properties *of MAB* phase nanolaminated ternary borides: M_2AlB_2 (M = Mn, Fe and Co) under spin effects

Gokhan Surucu [a, b, *], Bugra Yildiz [c], Aytac Erkisi [d], Xiaotian Wang [e], Ozge Surucu [f]

[a] Middle East Technical University, Department of Physics, Ankara, 06800, Turkey
[b] Department of Electric and Energy, Ahi Evran University, Kirsehir, 40100, Turkey
[c] Hacettepe University, Department of Physics Engineering, Ankara, 06800, Turkey
[d] Pamukkale University, Department of Physics, Denizli, 20020, Turkey
[e] School of Physical Science and Technology, Southwest University, Chongqing, 400715, China
[f] Department of Electrical and Electronics Engineering, Atilim University, Ankara, 06836, Turkey

ARTICLE INFO

Article history:
Received 5 February 2020
Received in revised form
20 April 2020
Accepted 29 April 2020
Available online 16 May 2020

Keywords:
MAB phases
Nanolaminated ternary borides
Spin effect
Anisotropic elastic
Density functional theory

ABSTRACT

In the present study, the structural, electronic, magnetic, anisotropic elastic and lattice dynamic properties of the ternary metal borides M_2AlB_2 (M = *Mn*, *Fe* and *Co*) known as *MAB* phases have been investigated by density functional theory. The obtained results from the structural optimizations show that all these compounds have negative formation enthalpy implying the thermodynamic stability and synthesizability. The spin effects on the M_2AlB_2 phases have been studied with the plotted energy-volume curves for different magnetic phases (antiferromagnetic (*AFM*), ferromagnetic (*FM*), and paramagnetic (*PM*)) of these compounds. The stable magnetic phase for the Mn_2AlB_2 compound is found to be *AFM* while the magnetic nature of Fe_2AlB_2 and Co_2AlB_2 compounds are *FM*. The calculated electronic band structures with the total and orbital projected partial density of electronic states imply that these ternary metal borides have metallic behavior. Also, the mentioned compounds have mechanical and dynamic stability due to the calculated elastic constants and the observed phonon dispersion curves. Some thermodynamic properties have been investigated by means of phonon dispersion curves. Furthermore, the anisotropic elastic properties have been visualized in three dimensions (3D) for Young's modulus, linear compressibility, shear modulus, Poisson's ratio, and sound wave velocities.

1. Introduction

The fascinating mechanical, electrical, and magnetic properties, and radiation damage tolerance make nanolaminated materials the promising candidates for the possible applications in future energy, transportation, and defense technologies [1]. The most well-known nanolaminates are the so-called MAX phases. The general formula of *MAX* phases are given as $M_{n+1}AX_n$ n = 1, 2 or 3 (where M is a transition metal, A is a group A element, and X is either carbon or nitrogen) and these are usually known as nanolaminated materials in which *MX* slabs with strong *M-X* bonds are separated by *A*-layers with weaker *M-A* bonds [2]. *MAX* phases have outstanding properties such as high thermal and mechanical stability, good thermal and electrical conductivity with hardness, stiffness and brittleness nature. Hence, *MAX* phases could be considered as metallic ceramics [3–5].

Ternary metal borides called *MAB* phases, was first discovered experimentally by Ade and Hillebrecht, also exhibit nanolaminated structure [6]. Having similar physical properties with *MAX* phases make *MAB* phases popular. Lu et al. carried out the study about the structural analysis of nanolaminated $AlCr_2B_2$ and $AlFe_2B_2$ compounds which are the *MAB* phases [7]. In particular, some experimental studies on the usage of $AlFe_2B_2$ compound as magnetocaloric material have led to rise in the interest in these types of structures [8,9]. Nanolaminated Mn_2AlB_2 compound was also experimentally studied in terms of their magnetic orders [10].

Also, in literature, there are some studies about transition metal borides as regarded ultrahigh temperature and hypersonic

* Corresponding author. Middle East Technical University, Department of Physics, Ankara, 06800, Turkey.
E-mail address: info@gokhansurucu.com (G. Surucu).

https://doi.org/10.1016/j.jallcom.2020.155436
0925-8388/

ceramics [11–13]. Hence, the mechanical properties of these materials are important for technological and industrial applications. The elastic properties of *AlCrB* and $AlFe_2B_2$ were investigated by Nie et al. [14] and Cheng et al. [15], respectively. Moreover, there are many reported studies on the mechanical properties, magnetic and electronic behavior of ternary transition metal borides [16–27].

Hardness and high melting temperature, which are some of the mechanical and thermodynamic properties of a solid, are very important parameters due to use for coatings in many industrial applications. The early (i.e., groups 3 and 4), middle (i.e., groups 5, 6, and 7) or late transition metals (i.e., groups 8, 9, 10, and 11) based borides and carbides are considered as the hardest and highest melting compounds [28–30]. In some recent studies, it was shown that some compounds such as ReB_2 and OsB_2 have remarkable hardness and low compressibility due to have a strong covalent bonding between boron atoms and a strong repulsion between the core electrons of the 5d metal [31–33]. In this context, the discovery of particularly interesting mechanical properties of the borides of this transition metal element group is the main source of motivation in this study.

In the literature there are few works about structural and mechanical properties of Mn_2AlB_2, Co_2AlB_2 *and* Fe_2AlB_2 compounds as discussed above. In addition, there are very limited study about each M_2AlB_2 (M = *Mn*, *Fe* and *Co*) phases in terms of their mechanical, lattice dynamical and electronic properties, and the spin effects on these properties. This work presents the detailed theoretical study that covers the structural, electronic, magnetic, anisotropic elastic and lattice dynamical properties of each ternary metal borides M_2AlB_2 (M = *Mn*, *Fe* and *Co*).

2. Computational details

In this study, all of the calculations have been carried out by DFT (Density Functional Theory), as implemented in the VASP (Vienna AB Initio Simulation Package) [34–36]. To approximate exchange-correlation potential within the framework of spin-polarised generalized gradient approximation (GGA) [37], the Perdew, Burke and Ernzerhof (PBE) [38] type pseudopotentials have been used. For *Mn*, *Fe*, *Co*, *Al* and *B* atoms in the compositions, the valance electron configurations are $4s^1\ 3d^5$, $4s^2\ 3d^6$, $4s^2\ 3d^7$, $3s^2\ 3p^1$ and $2s^2 2p^1$, respectively. The interactions between the ion cores and valence electrons have been described under the Projector-augmented wave (PAW) method. The reciprocal space has been sampled by 16 x 4 x 16 M − P (Monkhorst-Pack) scheme [39], and the energy cut-off for the plane wave basis set has been fixed at 550 eV. The ionic positions of atoms and the cell volume by setting ISIF = 3 has been used as implemented in the VASP code [34–36] for M_2AlB_2 (M = *Mn*, *Fe* and *Co*) compounds. The positions of the atoms have been fully relaxed until the maximum force on each atom became smaller than 10^{-11} eV/Å and Methfessel-Paxton smearing method has been used with 0.01 eV smearing width. The energy tolerance is less than 10^{-10} eV per unit cell in the iterative solution of the Kohn-Sham equations. The elastic constants have been calculated with the "stress−strain" approximation as implemented in VASP uses IBRION = 6 and ISIF = 3 parameters [40]. The anisotropic elastic properties have been obtained by using ELATE [41] and Christoffel [42] programs where the calculated elastic constants have been employed. The vibrational properties have been studied by VASP using linear response method with the supercell approach (3 × 1 × 3 supercell) which is generated using the PHONON software [43]. The crystal structures and the visualization have been shown by using VESTA [44].

3. Results and discussion

Firstly, these materials have been optimized until all the forces and pressures become zero in the primitive cell to detect the most suitable atomic positions in our systems and obtain some structural parameters. M_2AlB_2 compounds have orthorhombic crystal structure and conform to *Cmmm* space group having 65 space number. Fig. 1 illustrates the three-dimensional crystallographic shapes of M_2AlB_2 compounds in which two *Al* atoms are placed at *2c* (*0.5*, *0*, *0.5*) Wyckoff positions [45], four transition metal (M) atoms (*Mn*, *Fe* and *Co*) are positioned on *4i* (*0*, *0.146*, *0*). The four B atoms in the M_2AlB_2 compounds are located at *4j* (*0*, *0.294*, *0.5*) for Mn_2AlB_2 and Fe_2AlB_2 crystals, while the *B* atoms in Co_2AlB_2 are placed in *4j* (*0*, *0.293*, *0.5*). After the optimization process, the formation enthalpies have been calculated to determine the thermodynamic stability and structural synthesizability for each M_2AlB_2 compounds. Then, the electronic nature in most suitable magnetic phase, elasticity and mechanical stability, lattice dynamical and some thermal properties have been investigated by using these optimized parameters.

3.1. The structural properties in different magnetic orders

The formation enthalpy value (ΔH_f) which can be calculated by using internal energy changes [46] as given in Eq. (1), is much important parameter indicating the structural and thermodynamic stability of a crystal. This value, for a bulk crystal having A_xB_y chemical formula, can be calculated by;

$$\Delta H_f = E_{tot} - \left(xE_A^{bulk} + yE_B^{bulk}\right) \quad (1)$$

where, E_A^{bulk} and E_B^{bulk} are the ground state energies for *A* and *B* atoms and E_{tot} is the total energy of the unit cell.

To investigate magnetic orders of the M_2AlB_2 compounds and the spin effects on these compositions, the spin directions of the atoms in the unit cell have been changed. The calculated formation enthalpies of the M_2AlB_2 compounds in ferromagnetic, antiferromagnetic and paramagnetic orders have been given in Table 1 and, it is obviously seen from the calculated formation enthalpies that the most suitable magnetic phase is *AFM* for Mn_2AlB_2 compound while Fe_2AlB_2 and Co_2AlB_2 compounds have *FM* nature. Also, these determined magnetic orders for the M_2AlB_2 compounds are in consistent with the literature [2,7–10,14–27]. Then, the total energies of the unit cell as a function of volume in ferromagnetic, antiferromagnetic and paramagnetic phases are given in Fig. 2. As shown in Fig. 2, after securing ground state energy-volume values, these values have been normalized and plotted by using Vinet equation to determine the ferromagnetic (FM), antiferromagnetic (AFM) or paramagnetic (PM) nature of these compounds [47]. Fig. 2 also illustrates that the energetically more favored magnetic phase of Mn_2AlB_2 compound is AFM phase. When compared to the experimental result from the literature by Potashnikov et al. [10], the determined result for Mn_2AlB_2 with this study has the same tendency. On the other hand, as seen from Fig. 2 that the more favored magnetic phase of Fe_2AlB_2 and Co_2AlB_2 compounds are FM phase. By taking into consideration of the literature, for Fe_2AlB_2 and Co_2AlB_2 compounds, the some experimental studies [7,8,15,20,21,27] indicated that *FM* phase was the most favored phase among the all other magnetic phases. Hence, the obtained magnetic order tendency results for M_2AlB_2 compounds in this study are consistent with the literature.

In Table 1, the lattice parameters (a, b, c) and bond lengths (d) obtained during the optimization process have been tabulated for the most stable magnetic phase. When compared the calculated

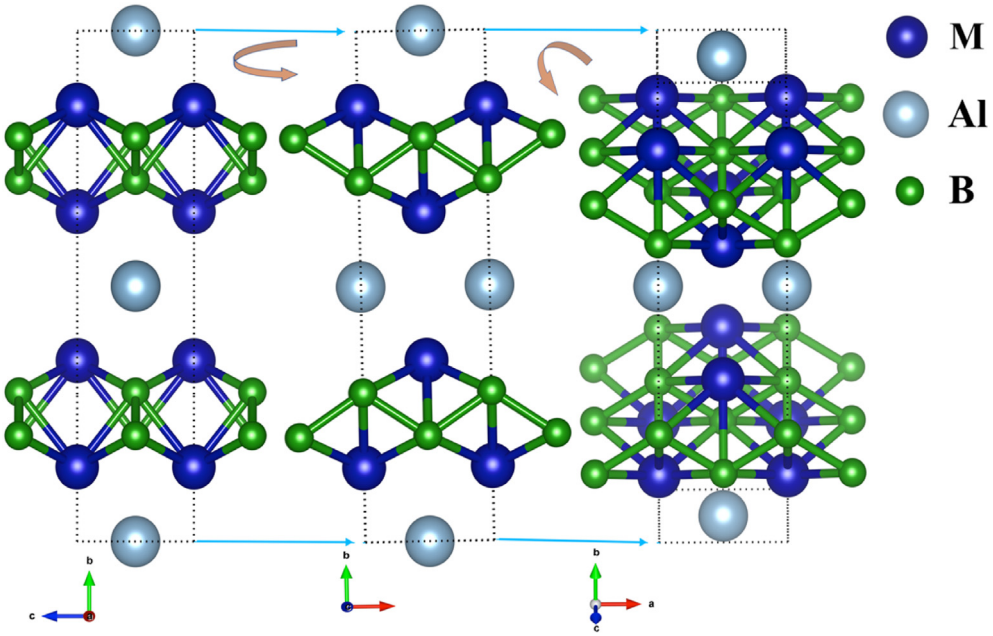

Fig. 1. The three-dimensional (3D) crystallographic shape of primitive cell modeled by 10 atoms of nanolaminated ternary borides M_2AlB_2 (M = *Mn*, *Fe* and *Co*) in different views.

Table 1
The calculated formation enthalpies (ΔH_f in *eV/f.u.*) of nanolaminated ternary borides M_2AlB_2 (M = *Mn*, *Fe* and *Co*) in three different type magnetic orders, where f.u. is formula unit, and also, the optimized lattice parameters (*a*, *b*, *c in* Å) and bond lengths (*d in* Å) in the most stable magnetic phase.

Compound	a	b	c	d_{M-Al}	d_{M-B}	ΔH_f
Mn_2AlB_2	2.894	11.070	2.828	2.584	2.133	−0.406 (A*FM*)
						−0.403 (*FM*)
						−0.403 (*PM*)
	2.894 [2]	11.070 [2]	2.830 [2]			−0.333 [2]
	2.923 [2]	11.070 [2]	2.899 [2]			
	2.936 [22]	11.120 [22]	2.912 [22]			
Fe_2AlB_2	2.915	11.021	2.855	2.601	2.145	−0.395 (A*FM*)
						−0.405 (*FM*)
						−0.345 (*PM*)
	2.916 [2]	11.022 [2]	2.851 [2]			−0.538 [2]
	2.925 [2]	11.027 [2]	2.865 [2]			
	2.928 [7]	11.032 [7]	2.869 [7]			
	2.928 [8]	11.033 [8]	2.868 [8]			
	2.917 [9]	11.010 [9]	2.864 [9]			
	2.919 [9]	10.989 [9]	2.880 [9]			
	2.905 [15]	10.954 [15]	2.827 [15]			
	2.924 [20]	11.033 [20]	2.870 [20]			
	2.931 [21]	11.028 [21]	2.861 [21]			
	2.945 [22]	11.090 [22]	2.887 [22]			
	2.929 [23]	11.039 [23]	2.867 [23]			
Co_2AlB_2	2.964	11.320	2.688	2.594	1.769	−0.317 (A*FM*)
						−0.318 (*FM*)
						−0.317 (*PM*)
	2.965 [2]	11.330 [2]	2.683 [2]			0.130 [2]

lattice parameters for Mn_2AlB_2, Fe_2AlB_2 and Co_2AlB_2 compounds with the results from the literature [2,7–9,15,20–23] as given in Table 1, it has been clearly seen that the present lattice parameters are in agreement with the theoretical and experimental ones.

Additionally, M_2AlB_2 compounds are thermodynamically stable and synthesizable with negative formation energies. Although the formation enthalpy (ΔH_f) of Co_2AlB_2 compound was found to be positive in the study of Kadas et al. [2], this value was calculated as negative in this study. This discrepancy could be form due to the calculation of the formation enthalpies with different methods. Moreover, the bond lengths between transition metal atoms and aluminum atoms are larger than the bond-lengths between transition metal atoms and boron atoms as given in Table 1.

For the solid crystals having magnetic properties, the Curie temperature (T_c) is a critical and vital parameter. At this temperature, certain materials lose their permanent magnetic properties, to be replaced by induced magnetism, and, as given in Eq. (2), which can be roughly estimated from mean field approximation [48,49] by using the ground state energy difference (ΔE) between antiferromagnetic and ferromagnetic phase,

$$T_c = \frac{2}{3k_B}\Delta E \tag{2}$$

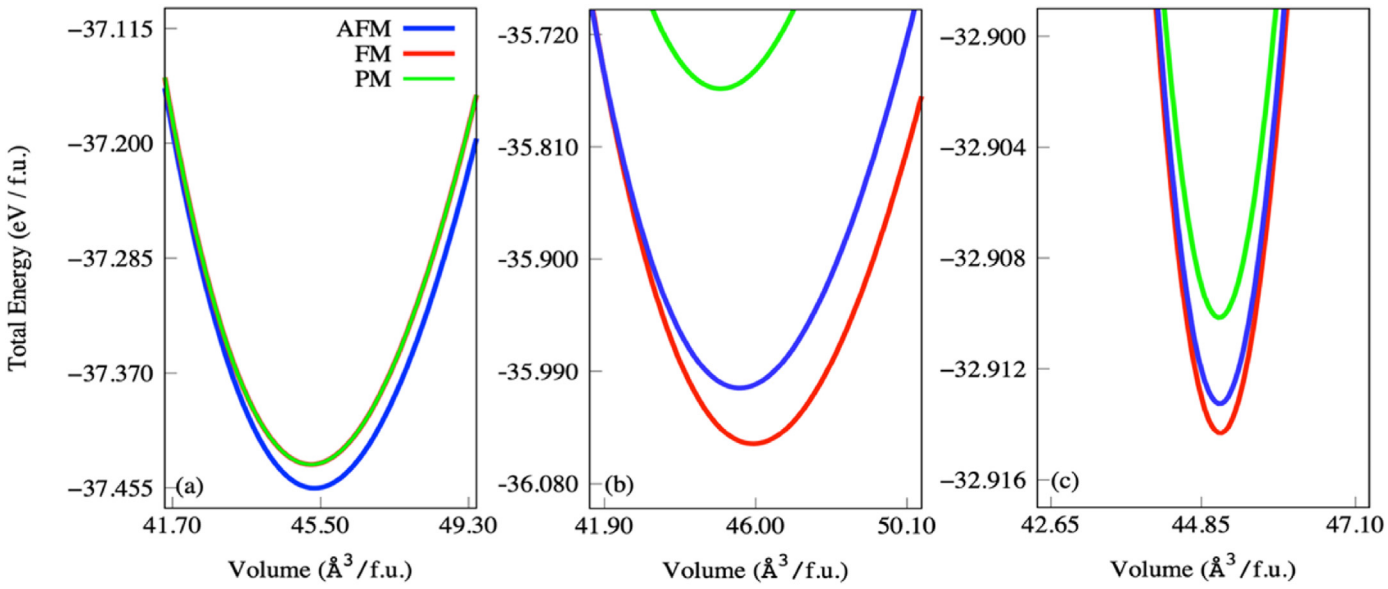

Fig. 2. Total energies of the unit cell as a function of volume in ferromagnetic, antiferromagnetic and paramagnetic phases of (a) Mn_2AlB_2, (b) Fe_2AlB_2 and (c) Co_2AlB_2 where f.u. is formula unit.

where k_B is Boltzman constant. The calculated ground state energy differences between ferromagnetic and antiferromagnetic phases and the estimated Curie temperatures for the nanolaminated ternary borides M_2AlB_2 (M = *Mn*, *Fe* and *Co*) have been tabulated in Table 2. The calculated Curie temperature of Mn_2AlB_2 and Fe_2AlB_2 compounds have been found to be around the room temperature and this value is in a good agreement with the experimental [22,23] and the theoretical [27] studies from the literature. In addition, about the room temperature, the magnetic properties of Mn_2AlB_2 and Fe_2AlB_2 compounds are not be suppressed. Hence, it could be deduced that these compounds are suitable for spintronic applications [50]. The partial magnetic moments of atoms in crystals are vital to understand which atoms play a more effective role in the magnetic nature of the compounds. In this regard, the calculated partial magnetic moments (μ_{atom}) of atoms show that transition metal atoms (M = *Mn*, *Fe* and *Co*) in the nanolaminated ternary borides (M_2AlB_2) have great responsibility for the magnetic behavior in these materials. The calculated total and partial magnetic moments (μ_B) of these compounds have been tabulated in Table 2. It can be clearly seen that the obtained total and partial magnetic moments of M_2AlB_2 compounds are in a good agreement with the experimental [2,9,10] and the theoretical [2,27] studies from the literature. Moreover, the partial magnetic moment values show that the dominantly contributions to the magnetic properties come from the 3d substitutions on M sites in the M_2AlB_2 compounds.

3.2. The observed electronic behavior in favorable magnetic phase

On the basis of the derived equilibrium lattice constants and the energetically favorable magnetic phase, the electronic band structures of M_2AlB_2 (M = *Mn*, *Fe* and *Co*) compounds has been calculated. For the M_2AlB_2 compounds, the obtained spin-polarised band structures and the corresponding total density of states (TDOS) plotted along the high symmetry points in the first Brillouin zone have been illustrated in Fig. 3a-c. It is evident from these figures

Table 2
The calculated ground state energy values for antiferromagnetic (E_{AFM} in eV) and ferromagnetic (E_{FM} in eV) orders, predicted Curie temperatures (T_C in K), total and partial magnetic moments (μ_B) of nanolaminated ternary borides M_2AlB_2 (M = *Mn*, *Fe* and *Co*).

Compound	E_{AFM}	E_{FM}	T_C	$\mu_B/f.u$	$\mu_B/atom$		
					M	Al	B
Mn_2AlB_2	−37.456	−37.419	291	0.834	0.430	−0.002	−0.011
				0.820 [2]			
				0.750 [2]			
				0.710 [10]			
			296 [27]				
Fe_2AlB_2	−36.008	−36.046	294	2.808	1.422	−0.004	−0.014
				2.700 [2]			
				2.670 [2]			
					1.400 [9]		
			282 [22]				
			274 [23]				
			298 [27]	2.730 [27]	1.430 [27]	−0.004 [27]	−0.010 [27]
Co_2AlB_2	−32.913	−32.914	12	0.356	0.179	0.000	−0.001
				0.310 [2]			
				0.390 [2]			
					0.200 [27]		

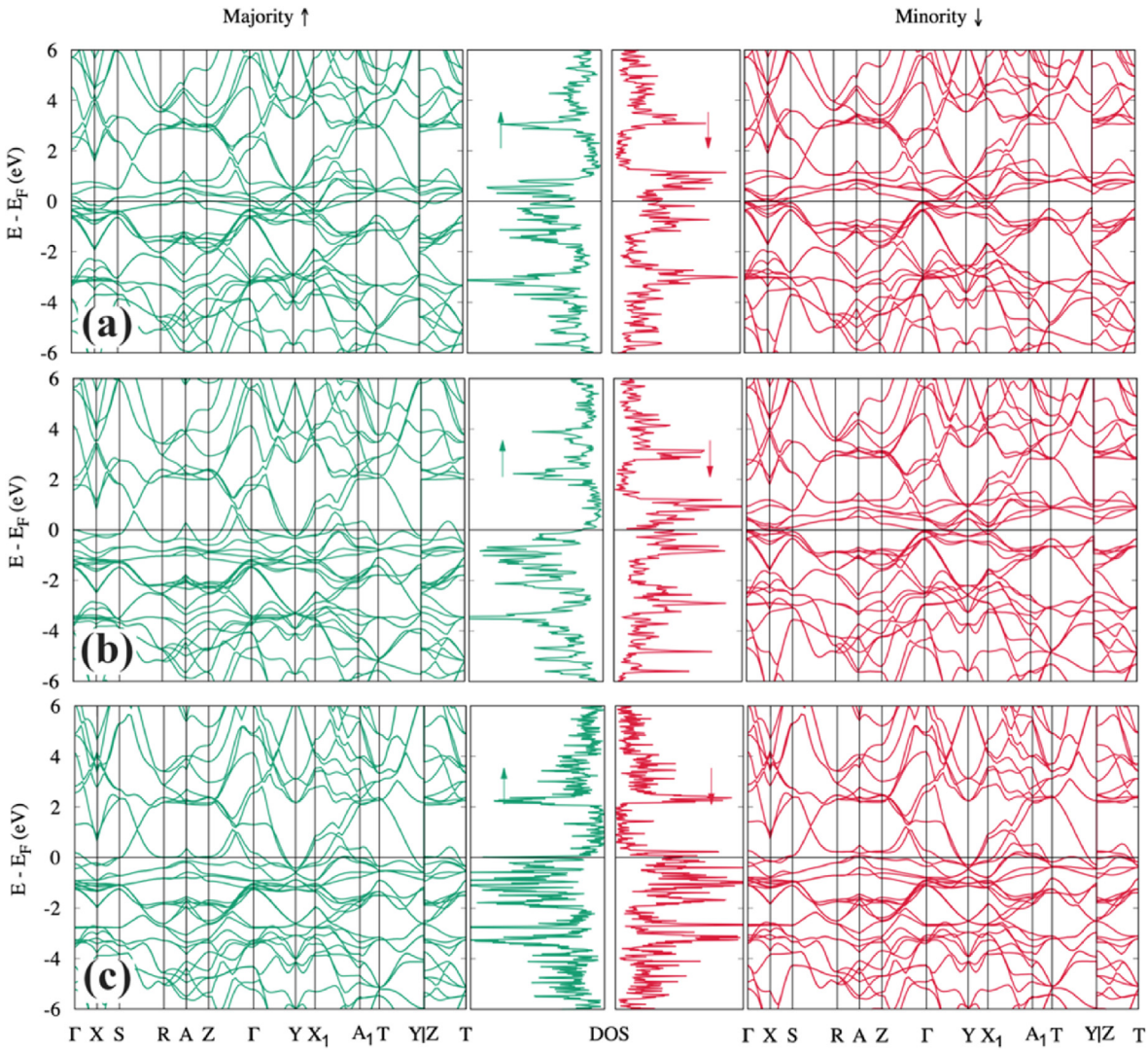

Fig. 3. Electronic band structure with the corresponding TDOS for (a) Mn_2AlB_2, (b) Fe_2AlB_2 and (c) Co_2AlB_2. The zero of band energy is shifted to Fermi level (E_F).

that all three compounds have metallic character because there is no band gap around the Fermi energy level in both spin states. Also, the lack of full symmetry between the majority and minority spin channels indicates that all three materials are not paramagnetic. In addition to the plotted electronic band structures, the orbital projected partial density of states (PDOS) and total density of states (TDOS) have been calculated, as presented in Fig. 4a-c, for Mn_2AlB_2, Fe_2AlB_2 and Co_2AlB_2 compounds, respectively. As seen from these figures, there are strong hybridizations between the d-orbitals of the transition metal atoms (*Mn*, *Fe* and *Co*) and the p-states of the aluminum and boron atoms especially around Fermi level. In addition, there are strong hybridizations between *d*-orbitals of transition metal atoms (*Mn*, *Fe* and *Co*) and *p*-states of aluminium and boron atoms. The hybridizations exist between the states of the *3p*-states and *2p*-states of aluminium and boron atoms and *3d*-states of transition metal atoms, both below the Fermi level (almost between −3 eV and −6 eV), known as the valence band, and above the Fermi level (almost between 2.5 eV and 6 eV), known as the conduction band. For all three compositions, the dominance of the *d*-states of the transition metal atoms can be clearly understood from the plotted orbital projected partial density of states. This means that, d-orbitals of *Mn*, *Fe* and *Co* atoms are mainly responsible for the metallic character of these crystals and also have significant contributions on the formation of the materials and chemical bonding. Also, to understand the chemical bonding type made by atoms, two-dimensional electron-density distributions have been plotted for different plane is shown in Fig. 5. These plots indicate that transition metal atoms (*Mn*, *Fe* and *Co*) and aluminium (*Al*) atoms make ionic bonds whereas boron (*B*) atoms make covalent bonds with each other. Hence, the TDOS and PDOS of M_2AlB_2 compounds have been found to be well compatible with previous theoretical study in the literature [2,9,27].

3.3. The prediction of elasticity properties and the determination of mechanical stability

The mechanical stability and the elastic properties are very crucial for various industrial applications. In order to understand the flexibility and mechanical stability of M_2AlB_2 (M = Mn, Fe and Co) compounds, the elastic constants (C_{ij}), which are nine independents constants for an orthorhombic crystal, have been calculated using the stress-strain approach [51], as seen in Table 3. The mechanical stability of a material can be determined by the Born's stability criteria's [52]. For any solid crystal having

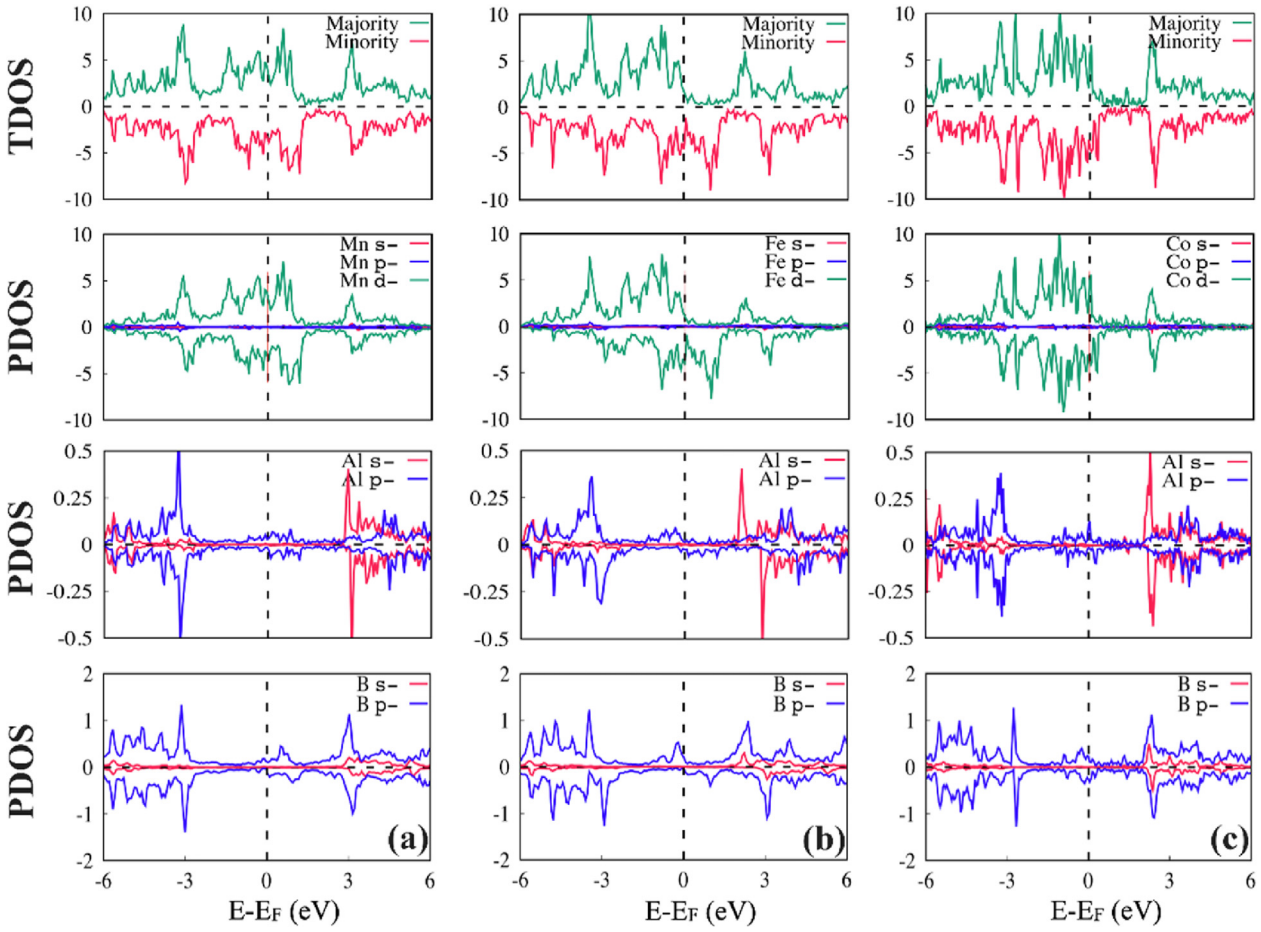

Fig. 4. The TDOS and the PDOS in the compositions for (a) Mn_2AlB_2, (b) Fe_2AlB_2 and (c) Co_2AlB_2.

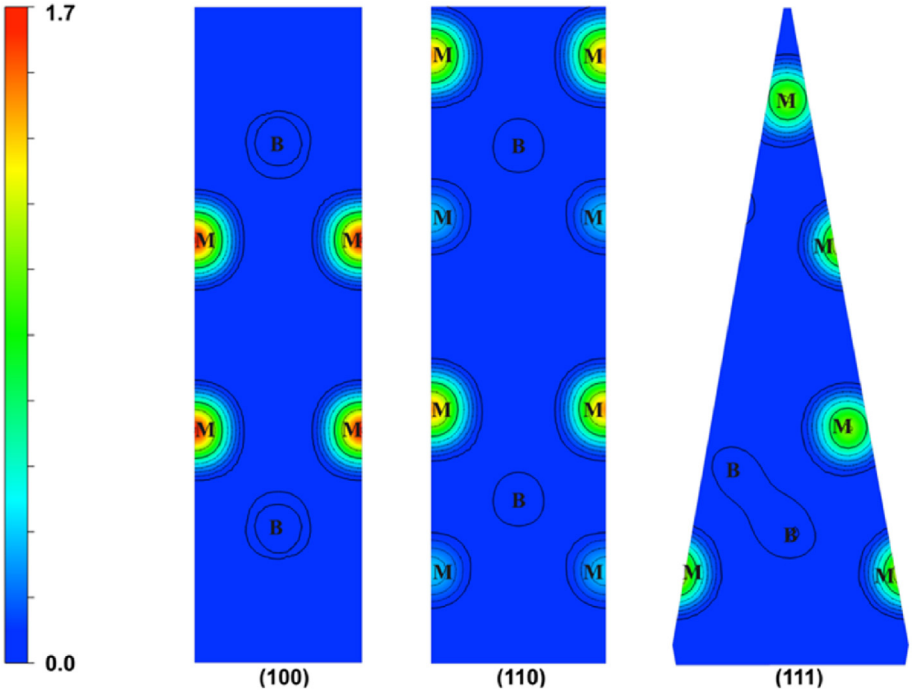

Fig. 5. The 2D (two-dimensional) Electron-density distribution (in units of e) for the nanolaminated ternary borides M_2AlB_2 (M = *Mn*, *Fe* and *Co*) in different plane.

Table 3
The calculated elastic constants (C_{ij} in GPa) for nanolaminated ternary borides M_2AlB_2 (M = *Mn*, *Fe* and *Co*).

Compound	C_{11}	C_{12}	C_{13}	C_{22}	C_{23}	C_{33}	C_{44}	C_{55}	C_{66}
Mn_2AlB_2	467.5	172.4	105.1	342.8	94.8	459.7	154.7	195.9	170.4
	486.0 [2]	193.5 [2]	132.1 [2]	413.1 [2]	140.0 [2]	478.0 [2]	152.2 [2]	192.2 [2]	186.9 [2]
Fe_2AlB_2	426.2	148.7	120.4	378.6	132.9	307.4	132.4	168.0	134.8
	447.0 [2]	170.1 [2]	133.9 [2]	402.7 [2]	156.4 [2]	334.6 [2]	140.2 [2]	166.3 [2]	156.2 [2]
	389.1 [14]	138.7 [14]	128.7 [14]	433.2 [14]	118.3 [14]	348.7 [14]	171.4 [14]	137.5 [14]	141.2 [14]
Co_2AlB_2	371.8	180.0	165.7	303.6	165.2	274.1	107.8	155.8	85.8
	380.2 [2]	193.3 [2]	199.0 [2]	317.1 [2]	186.9 [2]	319.9 [2]	127.6 [2]	153.1 [2]	102.2 [2]

orthorhombic structure, the mechanical stability conditions have been given as;

$$C_{ii} > 0 \; and \; (C_{ii} + C_{ij} - 2C_{ij} > 0) \; for \quad i = 1 \ldots 6 \tag{3}$$

It can be easily understood from the Table 3 that these materials are mechanically stable since they meet the Born's stability criteria. The comparison of the obtained results revealed that the calculated elastic constants (C_{11}, C_{33}, C_{44} and C_{55} values) are coherent, while C_{12}, C_{13}, C_{22}, C_{23} and C_{66} values are higher (about 8–30%) than the theoretical values in literature [2] for Mn_2AlB_2 compounds. Moreover, when compared the calculated elastic constants for Fe_2AlB_2 with the calculated results in Ref. [2,14] and for Co_2AlB_2 with the calculated results in Ref. [2] there are difference about 1–20% and 2–16%, respectively. The differences could be originated from the usage of different calculation techniques. In addition, once compared the C_{11}, C_{22} and C_{33}, C_{11} has the largest value among the other elastic constants for M_2AlB_2 compounds. This result indicates that M_2AlB_2 compounds are harder to compress along *a-axis* which has strong B–B bonds (see Fig. 1). Also, the trend observed for C_{11}, C_{22} and C_{33} is coherent with the study of Kadas et al. [2].

3.3.1. The prediction of anisotropic elastic properties

The mechanical properties such as bulk (B), shear (G) and Young's (E) modulus, Pugh's (B/G) and Poisson's (σ) ratios, hardness (H) and anisotropy parameters (A_1, A_2 and A_3) have been estimated by using the calculated elastic constants [53]. Voigt [54], Reuss [55] and Hill [56] approaches have been used for upper, lower and average values as seen in Eqs. (4)–(7).

$$B_V = (1/9)[C_{11} + C_{22} + C_{33} + 2(C_{12} + C_{13} + C_{23})] \tag{4}$$

$$B_R = [(S_{11} + S_{22} + S_{33}) + 2(S_{12} + S_{13} + S_{23})]^{-1} \tag{5}$$

$$G_V = (1/15)[C_{11} + C_{22} + C_{33} - (C_{12} + C_{13} + C_{23}) + 3(C_{44} + C_{55} + C_{66})] \tag{6}$$

$$G_R = 15[4(S_{11} + S_{22} + S_{33}) - 4(S_{12} + S_{13} + S_{23}) + 3(S_{44} + S_{55} + S_{66})]^{-1} \tag{7}$$

where S_{ij} elastic compliance constants for an orthorhombic crystal. For a solid crystal, the average of bulk (B) and shear moduli (G) can be defined as a measure of resistance to reversible deformations upon shear stress and represent the resistance to plastic deformation and these values have been calculated from $B = (B_V + B_R)/2$ and $G = (G_V + G_R)/2$ by using Hill approximation. In addition, other elastic properties, such as Young's moduli (E) and Poisson's ratios (σ), have been predicted by using Bulk and Shear modules, as given in Eq. (8). These values have been tabulated in Table 4.

Table 4
The estimated average values of bulk (B in GPa) and shear moduli (G in GPa), Young's moduli (E in GPa), Poisson's ratios (σ), Pugh's ratios (B/G) and also Vickers hardness (H_V in GPa), for nanolaminated ternary borides M_2AlB_2 (M = *Mn*, *Fe* and *Co*).

Compound	B	G	E	B/G	σ	H_V
Mn_2AlB_2	221.6	160.6	388.0	1.38	0.21	10.26
	256.0 [2]	164.8 [2]	407.1 [2]	1.55 [2]	0.23 [2]	7.30 [2]
Fe_2AlB_2	210.5	132.5	328.7	1.59	0.24	9.54
	231.8 [2]	138.8 [2]	347.2 [2]	1.67 [2]	0.25 [2]	9.50 [2]
						10.20 [26]
Co_2AlB_2	216.8	94.5	247.5	2.29	0.31	8.87
	240.5 [2]	101.0 [2]	265.9 [2]	2.38 [2]	0.32 [2]	

$$E = \frac{9GB}{G + 3B} \; , \nu = \frac{3B - 2G}{2(G + 3B)} \tag{8}$$

Among the elastic properties, the Young moduli, which can be defined as ratio of stress and strain and can give information about linear strain along the edges of any solid crystal, is much important parameter since it can characterize the stiffness of materials. When the values in Table 4 are considered, these compounds can be classified as hard materials. Furthermore, Mn_2AlB_2 is stiffer than the others due to its highest E value while Co_2AlB_2 has highest flexibility due to its lowest value.

By looking at the Poisson ratio of a crystal, a determination can be made about its compressibility feature. For a solid crystal, when the Poission ratio approaches about 0.5, it can be classified as an incompressible material [57]. As given in Table 4, the calculated Poisson's ratio of these compounds is around 0.3, which means that they have almost compressible character. It is also known that the same ratio should be about 0.1 for covalent bonds and about 0.25 for ionic bonds [58]. Hence, it can be clearly seen that the type of binding between transition metal atoms (*Mn*, *Fe* and *Co*) and aluminium (*Al*) atoms in M_2AlB_2 compounds is closer to the ionic character. This type of binding is predominant especially in the Fe_2AlB_2 compound since the calculated ratio is much close to the critical value of 0.25.

Material's brittleness or ductility are another important mechanical property for the industrial applications. The Pugh's ratio [59] which can be calculated by using bulk and shear moduli of a crystal (B/G), gives so much information about elasticity of material. When the B/G ratio is higher than the critical value 1.75, material is said to be ductile. On contrary, if this ratio is lower than the critical value, material is said to be brittle. As can be inferred from Table 4, Mn_2AlB_2 and Fe_2AlB_2 are brittle materials while Co_2AlB_2 ductile.

The calculated hardness (H_V) values for M_2AlB_2 compounds have been calculated by using the semi-empirical method based on the electronegativities and covalent radii of the constituent atoms, and the bond lengths in the structure developed by Lyakhov et al. [60]. The calculated H_V values are also given in Table 4 and it has been concluded that Mn_2AlB_2 compound is the hardest material among the M_2AlB_2 compounds. In addition, the experimentally

Table 5
The calculated Cauchy pressures for the (100), (010), and (001) planes of nanolaminated ternary borides M_2AlB_2 (M = *Mn*, *Fe* and *Co*).

Compound	$C_{23}-C_{44}$ (*GPa*)	$C_{13}-C_{55}$ (*GPa*)	$C_{12}-C_{66}$ (*GPa*)
Mn_2AlB_2	−59.9	−90.8	2.00
Fe_2AlB_2	0.50	−47.6	13.9
Co_2AlB_2	57.4	9.90	94.2

obtained H_V value of Fe_2AlB_2 compound is well matched with the calculated value [26]. Due having no data about the Mn_2AlB_2 and Co_2AlB_2 compounds, the comparison could not be done for these compounds.

There is a relationship between the angular character of atomic bonding in a crystal and also its brittleness or ductility behavior. This relationship can be explained in detail using the calculated Cauchy pressure [60]. Having a large positive value of the Cauchy pressure indicates a ductile material with metallic bonds. In contrary, a negative value of the Cauchy pressure indicates a material having a brittle structure with a more angular bond character. A crystal with an orthorhombic structure may behave differently in all three crystallographic planes, unlike cubic systems that exhibit the same behavior in all planes. Therefore, the Cauchy pressures of an orthorhombic composition can be determined by the aid of elastic constants for three different planes; $C_{23}-C_{44}$ for the (100) plane, $C_{13}-C_{55}$ for the (010) plane, and $C_{12}-C_{66}$ for the (001) plane [61]. The calculated Cauchy pressures for different planes of M_2AlB_2 compounds have been tabulated in Table 5. As seen in this table, for the (100) plane, the calculated larger negative pressure value of Mn_2AlB_2 compound implies strong angular bonding character while the atomic bonding type of Co_2AlB_2 compound has strongly metallic character in the same plane. For the (010) plane, the calculated larger negative values of Mn_2AlB_2 and Fe_2AlB_2 compounds indicate strong angular type of atomic bonding whereas all of three compounds have metallic bonding character in the (001) plane (see Table 5).

The shear anisotropy factor in an orthorhombic structure can be defined for {1 0 0}, {0 1 0} and {0 0 1} planes as given in Eq. (9) [62]. For these planes, the calculated shear anisotropy factors show that for the {1 0 0} plane only Fe_2AlB_2 compound has a nearly isotropic character, while for the {0 0 1} plane both Fe_2AlB_2 and Co_2AlB_2 have isotropic feature (see Table 6).

$$A_{\{100\}}=\frac{4C_{44}}{(C_{11}+C_{33}-2C_{13})}\ ,\ A_{\{010\}}=\frac{4C_{55}}{(C_{22}+C_{33}-2C_{23})}\ ,\ A_{\{001\}}=\frac{4C_{66}}{(C_{11}+C_{22}-2C_{12})} \tag{9}$$

In addition to the calculated anisotropy factors for the different planes, the isotropic nature of a crystal can be defined by the percent anisotropy factors (A_B and A_G) [63] and universal anisotropy factor (A^U) [64] by using the upper and lower limits of bulk and shear modulus, as given in Eq. (10).

$$A_B=\frac{B_V-B_R}{B_V+B_R}\times 100\%\ ,A_G=\frac{G_V-G_R}{G_V+G_R}\times 100\%,\ A^U=5\frac{G_V}{G_R}+\frac{B_V}{B_R}-6 \tag{10}$$

It is known that; the percent anisotropy factors (A_B and A_G) and universal anisotropy factor (A^U) of an isotropic crystal must be should be zero. The calculated factors imply the high anisotropic degree of the bulk and shear modulus of M_2AlB_2 compounds.

To make a further determination, the direction dependent Young's modulus, linear compressibility, shear modulus and Poisson's ratio have been plotted with the obtained several elastic constants of Fe_2AlB_2 in 2D and 3D by using the EIAM code [41] as given in Fig. 6 (to save a space, the corresponding figures of $Mn_2AlB_2$and Co_2AlB_2 compounds are given in supplementary file as Fig. 6.1.1 and Fig. 6.1.2, respectively). In Fig. 6, the green shapes correspond to minimum values of the given parameters and the blues shapes correspond to maximum values. It is concluded from the figure that Fe_2AlB_2 compound has an anisotropic property for Young's modulus, shear modulus and Poisson's ratio while it has an isotropic property for linear compressibility.

Table 6
The predicted shear anisotropy factors ($A_{\{100\}}$, $A_{\{010\}}$, $A_{\{001\}}$) for different crystallographic planes and the percent anisotropy factors (A_B and A_G) and universal anisotropy factor (A^U) of nanolaminated ternary borides M_2AlB_2 (M = *Mn*, *Fe* and *Co*).

Compound	$A_{\{100\}}$	$A_{\{010\}}$	$A_{\{001\}}$	A_B(%)	A_G(%)	A^U
Mn_2AlB_2	0.863	1.278	1.464	0.981	2.155	0.240
Fe_2AlB_2	1.075	1.599	1.063	1.123	1.373	0.162
Co_2AlB_2	1.371	2.520	1.087	1.031	4.895	0.536

In addition, the direction dependent sound wave velocities and the related enhancement factor are obtained by using Christoffel program [42] with quadruple precision which only requires the elastic stiffness constants and the density of medium. There are two types of sound wave velocities, namely, the longitudinal sound wave velocity (v_l), and the two transverse wave velocities (v_t), in two directions. Fig. 7 shows the calculated group wave velocities, phase wave velocities and enhancement factors for Fe_2AlB_2 compound (to save a space, the corresponding figures of $Mn_2AlB_2$and Co_2AlB_2 compounds are given in supplementary file as Fig. 7.1.1 and Fig. 7.1.2, respectively). The two secondary modes (Fast Secondary and Slow Secondary) correspond to the transverse wave velocities and the sing primary mode (Primary mode) is the longitudinal wave velocity. It has been observed that the group wave velocity has higher value in all axis for the slow secondary mode. The group wave velocity in fast secondary mode has the lowest value in c-direction while the group wave velocity in primary mode has the lowest value in b-axis. The phase wave velocity in slow secondary mode is low in all directions, the phase wave velocity in fast secondary mode is fast in a- and b-axis and the phase wave velocity in primary mode has highest value in a-direction. In addition, the enhancement factor in slow secondary mode has the highest value in b-axis. The enhancement factor in fast secondary mode has the highest values in all axis while the enhancement factor in primary mode has the lower values in all axis.

3.4. The lattice dynamic properties and the calculated thermal conductivities

The phonon dispersion curves have also very high importance for evaluating the material stability since the soft phonon modes can reflect the possible distortion in crystal. In the literature, there are no theoretical or experimental study about the phonon dispersion curves of M_2AlB_2 (M = *Mn*, *Fe* and *Co*) compounds. With this study, the phonon dispersion curves and phonon frequencies have been calculated by using the supercell approach with the linear response method to check the dynamical stabilities of M_2AlB_2 (M = *Mn*, *Fe* and *Co*) compounds. For these compounds, the obtained phonon dispersion curves with phonon DOS have been shown in Fig. 8. There are 30 branches in the phonon graph consisting of 3 acoustic and 27 optic branches with respect to having 10 atoms in the primitive cell. It can be clearly seen that the phonon dispersion curves have no imaginary frequencies (except Co_2AlB_2), indicating the dynamical stability of M_2AlB_2 compounds. As seen in

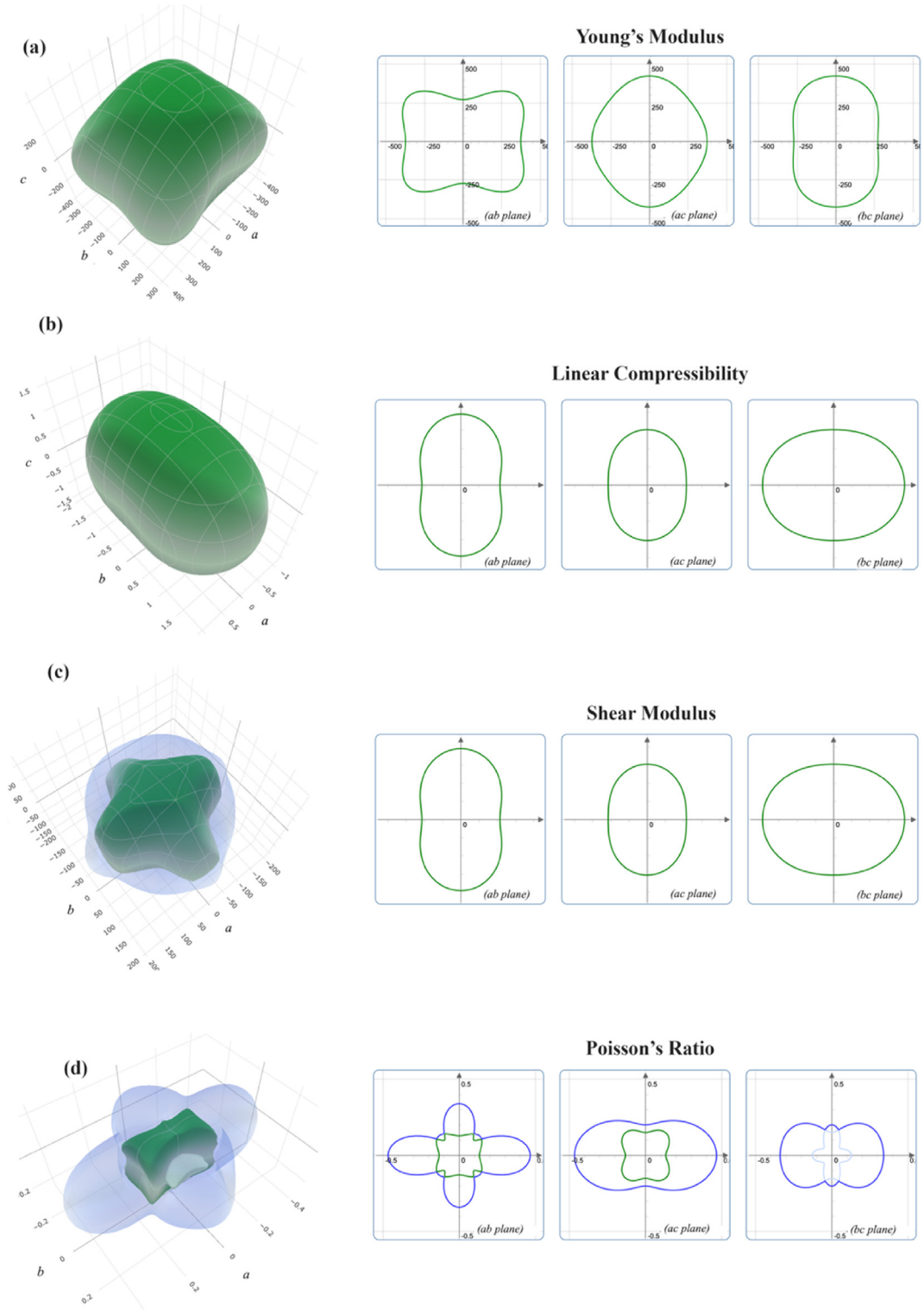

Fig. 6. The directional dependent (a) Young's modulus, (b) linear compressibility, (c) shear modulus and (d) Poisson's ratio of Fe_2AlB_2 compound.

Fig. 9, Co_2AlB_2 is dynamically unstable.

Hence, the lattice dynamical properties will be discussed in the text for Mn_2AlB_2 and $FeAlB_2$. When these graphics are analyzed together, it is seen that the sharp peaks in the phonon DOS come from the boron atoms and the transition metals (*Mn* and *Fe*). Explicitly, the dominant contribution to the acoustic branches originates from the *Mn* and *Fe* atoms. The optical modes (<12 THz) for Mn_2AlB_2 and $FeAlB_2$ are attributed to the vibrations of the *Al* atoms while the contribution at the higher frequencies (>12 THz) comes from the lightest element of the compound that is *B* atoms.

The thermal conductivities are much important and useful parameters for the technological applications such as thermal barrier coating. The observation of acoustic branches in the lower frequencies is the indication of low lattice thermal conductivity for the

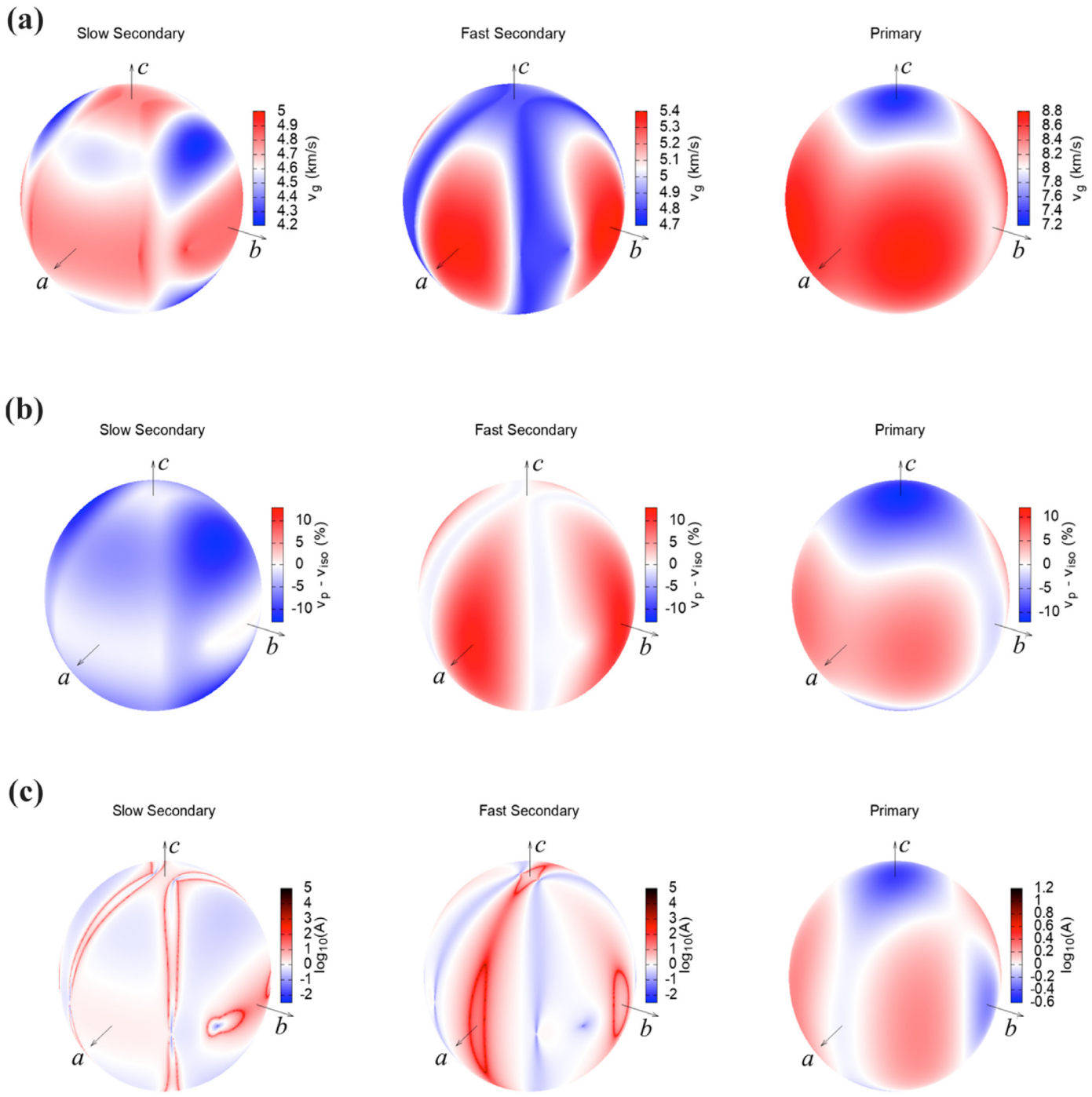

Fig. 7. (**a**) Group wave velocity, (**b**) phase wave velocity, and (**c**) enhancement factor for Fe_2AlB_2 in 3D.

phases [65]. The distance between the acoustic and the low frequency optic phonon branches becomes the closest for Fe_2AlB_2while this distance is the furthest for Mn_2AlB_2. This condition is related to the thermal conductivities. Hence, the relation in between thermal conductivities of these compounds could be given as follows: $Fe_2AlB_2 < Mn_2AlB_2$.

To detail the thermal conductivities of these compounds better, two models namely Cahill model [66] and Clarke model [67] have been used. The calculated minimum thermal conductivity values have been tabulated in Table 7. It is clearly seen from this table, Mn_2AlB_2 has highest and Fe_2AlB_2 has the lowest thermal conductivity as expected from Fig. 8.

Finally, in this study some thermal behaviors of nanolaminated ternary borides M_2AlB_2 ($M = Mn$ and Fe), which were defined by using quasi-harmonic Debye model [68], are presented. The observed thermal properties have been derived in between 0 and 1000 K temperature range. The free energy, entropy and heat capacity (C_v, at constant volume) as a function of temperature for Mn_2AlB_2 and Fe_2AlB_2 compounds have been shown in Fig. 9(a) and (b), respectively. As the temperature increases, the entropy increases while the free energy decreases. It is realized from the figure that the value of C_v increases very rapidly with the

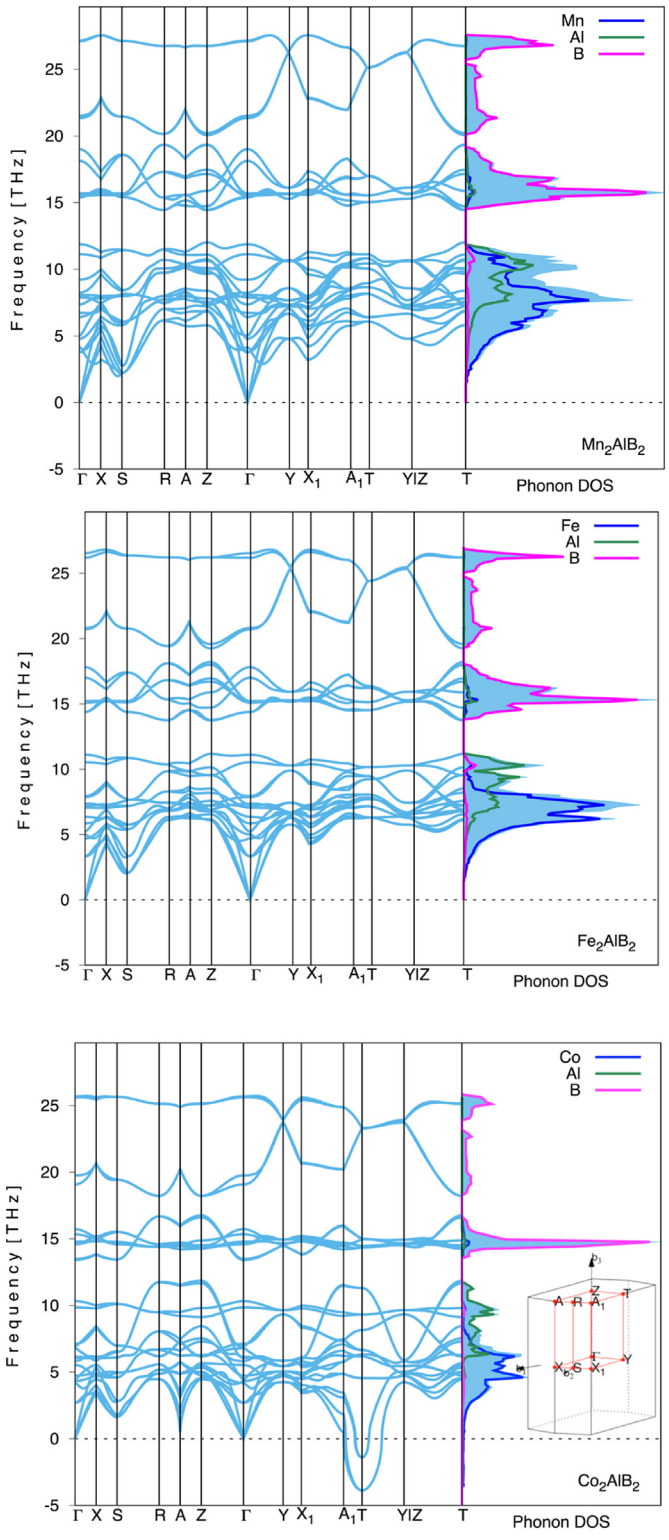

Fig. 8. The phonon dispersion curves with phonon DOS for nanolaminated ternary borides M_2AlB_2 (M = *Mn*, *Fe* and *Co*).

temperature until the temperature point *T*~400 K. Then the temperature above this point, the C_v increases slowly with the temperature and it almost approaches a constant value called as Dulong-Petit limit for these compounds.

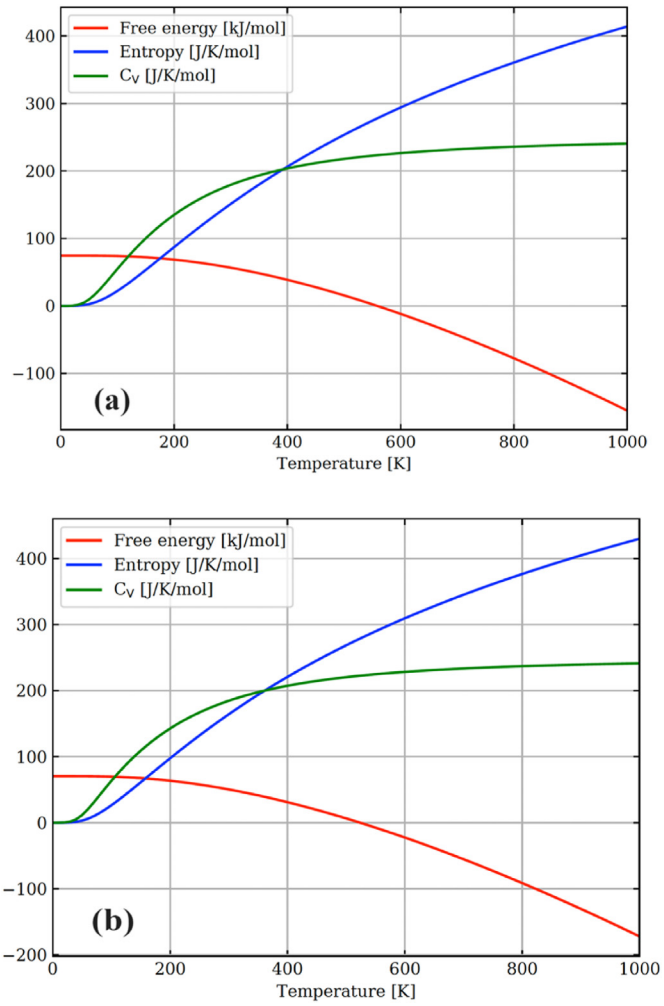

Fig. 9. The free energy, entropy and specific heat as a function of temperature of (a) Mn_2AlB_2 and (b) Fe_2AlB_2.

Table 7
The minimum thermal conductivities (λ_{min}) in Cahill and Clarke model for nanolaminated ternary borides M_2AlB_2 (M = *Mn*, *Fe* and *Co*).

Compounds	*Cahill model* λ_{min} ($W.m^{-1}.K^{-1}$)	*Clarke model* λ_{min} ($W.m^{-1}.K^{-1}$)
Mn_2AlB_2	2.456	2.258
Fe_2AlB_2	2.252	2.062

4. Conclusion

In this work, structural, electronic, mechanical, lattice dynamic and thermal properties have been studied in detail for the M_2AlB_2 (M = *Mn*, *Fe* and *Co*) compounds which are known as nanolaminated ternary metal borides called *MAB* phases. The calculated lattice parameters, optimal atomic positions, electronic behavior and magnetic nature have been found to be a good agreement with theoretical and experimental studies from the literature. It has been concluded that Mn_2AlB_2 is in the magnetic order of *AFM*, Fe_2AlB_2 is in *FM* order, and Co_2AlB_2 is in the magnetic order of weakly *FM*. And, the observed electronic band structures for all compounds have indicated that M_2AlB_2 are in metallic nature. The M_2AlB_2 compounds are predicted energetically and mechanically stable. In addition, the comparisons of the calculated elastic constants have

indicated that these compounds are harder to compress along *a-axis* which has strong *B—B* bonds. Also, Fe_2AlB_2 is said to be stiff while Mn_2AlB_2 material is ultra-stiff. Moreover, the phase wave velocity in slow secondary mode has found to be low in all directions, the phase wave velocity in fast secondary mode has found to be fast in a- and b-axis and the phase wave velocity in primary mode has found to be highest in a-direction. In addition, it is determined that Mn_2AlB_2 and Fe_2AlB_2 compounds are dynamically stable while Co_2AlB_2 is dynamically unstable. The minimum thermal conductivity values calculated from two different models have showed that Mn_2AlB_2 compound has highest thermal conductivity. Therefore, *MAB* phases, similar to the well-known *MAX* phases, could be an important candidate for many industrial applications such as *Li*-ion batteries, durable coatings, superconducting materials and spintronic devices.

Declaration of competing interest

The authors declare that they have no known competing financial interests or personal relationships that could have appeared to influence the work reported in this paper.

CRediT authorship contribution statement

Gokhan Surucu: Conceptualization, Methodology, Software, Formal analysis, Writing - review & editing. **Bugra Yildiz:** Data curation, Writing - original draft. **Aytac Erkisi:** Investigation, Writing - original draft. **Xiaotian Wang:** Conceptualization, Writing - review & editing. **Ozge Surucu:** Investigation, Writing - review & editing.

Acknowledgment

This research was supported by the Pamukkale University Research Project Unit [project number 2019BSP013].

Appendix A. Supplementary data

Supplementary data to this article can be found online at https://doi.org/10.1016/j.jallcom.2020.155436.

References

[1] J. Wang, Q. Zhou, S. Shao, A. Misra, Strength and plasticity of nanolaminated materials, Mater. Res. Letts. 5 (2017) 1—19.
[2] K. Kadas, D. Iusan, J. Hellsvik, J. Cedervall, P. Berastegui, M. Sahlberg, U. Jansson, O. Eriksson, *AlM_2B_2 (M =Cr, Mn, Fe, Co, Ni): a group of nanolaminated materials*, J. Phys. Condens. Matter 29 (2017) 155402.
[3] M.W. Barsoum, T. El-Raghy, *Synthesis and characterization of a remarkable ceramic: Ti_3SiC_2*, J. Am. Ceram. Soc. 79 (1996) 1953—1956.
[4] H. Yoo, M.W. Barsoum, T. El-Raghy, *Materials science: Ti_3SiC_2 has negligible thermopower*, Nature 407 (2000) 581—582.
[5] I.M. Low, *Advances In Science And Technology of $M_{n+1}AX_n$ Phases*, Woodhead Publishing Limited, Cambridge, U.K., 2012.
[6] M. Ade, H. Hillebrecht, *Ternary borides Cr_2AlB_2, Cr_3AlB_4, and Cr_4AlB_6: The first members of the series $(CrB_2)_nCrAl$ with n = 1, 2, 3 and a unifying concept for ternary borides as MAB-phases*, Inorg. Chem. 54 (2015) 6122—6135.
[7] J. Lu, S. Kota, M. Barsoum, L. Hultman, Atomic structure and lattice defects in nanolaminated ternary transition metal borides, Mater. Res. Lett. 5 (2016) 235—241.
[8] X. Tan, P. Chai, C.M. Thompson, M. Shatruk, *Magnetocaloric effect in $AlFe_2B_2$: Toward magnetic refrigerants from earth-abundant elements*, J. Am. Chem. Soc. 135 (2013) 9553—9557.
[9] J. Cedervall, M.S. Andersson, T. Sarkar, E.K. Delczeg-Czirjak, L. Bergqvist, T.C. Hansen, P. Beran, P. Nordblad, M. Sahlberg, *Magnetic structure of the magnetocaloric compound $AlFe_2B_2$*, J. Alloys Compd. 664 (2016) 784—791.
[10] D. Potashnikov, E.N. Caspi, A. Pesach, A. Hoser, S. Kota, L. Verger, M.W. Barsoum, I. Felner, A. Keren, O. Rivin, *Magnetic ordering in the nanolaminar ternary Mn_2AlB_2 using neutron and X-ray diffraction*, J. Magn. Magn Mater. 471 (2019) 468—474.
[11] W.G. Farenholtz, G.E. Hilmas, I.G. Talmy, J.A. Zaykoski, Refractory diborides of zirconium and hafnium, J. Am. Ceram. Soc. 90 (2007) 1347—1364.
[12] M.M. Opeka, I.G. Talmy, J.A. Zaykoski, Oxidation-based materials selection for 2000°C + hypersonic aerosurfaces: theoretical considerations and historical experience, J. Mater. Sci. 39 (2004) 5887—5904.
[13] D.M. van Wie, D.G. Drewry, E.D. King, C.M. Hudson, The hypersonic environment: required operating conditions and design challenges, J. Mater. Sci. 39 (2004) 5915—5924.
[14] L. Nie, W. Zhou, Y. Zhan, Theoretical investigation of the AlCrB orthorhombic ternary compounds, Comput. Theor. Chem. 1020 (2013) 51—56.
[15] Y. Cheng, Z. Lv, X. Chen, L. Cai, *Structural, electronic and elastic properties of $AlFe_2B_2$: first-principles study*, Comput. Mater. Sci. 92 (2014) 253—257.
[16] N.F. Chaban, I.U.B. Kuzma, *Ternary systems Cr-Al-B and Mn-Al-B*, neorg, Materials 9 (1973) 1908—1911.
[17] H.J. Becher, K. Krogmann, E. Peisker, *Uber das ternare Borid Mn_2AlB_2*, Z. Anorg. Allg. Chem. 344 (1966) 140—147.
[18] W. Jeitschko, *The crystal structure of Fe_2AlB_2*, Acta Crystallogr. Sect. B Struct. Crystallogr. Cryst. Chem. 25 (1969) 163—165.
[19] W. Jeitschko, Die kristallstruktur von MoAlB, Monatsh. Chem. 97 (1966) 1472—1476.
[20] M. Elmassalami, D.D.S. Oliveira, H. Takeya, *On the ferromagnetism of $AlFe_2B_2$*, J. Magn. Magn Mater. 323 (2011) 2133—2136.
[21] L.H. Lewis, R. Barua, B. Lejeune, *Developing magnetofunctionality: coupled structural and magnetic phase transition in $AlFe_2B_2$*, J. Alloys Compd. 650 (2015) 482—488.
[22] P. Chai, S.a. Stoian, X. Tan, P.a. Dube, M. Shatruk, *Investigation of magnetic properties and electronic structure of layered-structure borides AlT_2B_2 (T = Fe, Mn, Cr) and $AlFe_{2-x}Mn_xB_2$*, J. Solid State Chem. 224 (2015) 52—61.
[23] S. Hirt, F. Yuan, Y. Mozharivskyj, H. Hillebrecht, *$AlFe_{2-x}Co_xB_2$ (x = 0-0.30): T_C tuning through Co substitution for a promising magnetocaloric material realized by spark plasma sintering*, Inorg. Chem. 55 (2016) 9677—9684.
[24] S. Okada, K. Iizumi, K. Kudaka, K. Kudou, M. Miyamoto, Y. Yu, T. Lundstrom, *Single crystal growth of $(Mo_xCr_{1-x})AlB$ and $(Mo_xW_{1-x})AlB$ by metal Al solutions and properties of the crystals*, J. Solid State Chem. 133 (1997) 36—43.
[25] S. Kota, M. Agne, E. Zapata-Solvas, O. Dezellus, D. Lopez, B. Gardiola, M. Radovic, M.W. Barsoum, Elastic properties, thermal stability, and thermodynamic parameters of MoAlB, Phys. Rev. B 95 (2017) 144108.
[26] N. Li, Y. Bai, S. Wang, Y. Zheng, F. Kong, X. Qi, R. Wang, X. He, A.I. Duff, *Rapid synthesis, electrical, and mechanical properties of polycrystalline Fe_2AlB_2 bulk from elemental powders*, J. Am. Ceram. Soc. 100 (2017) 4407—4411.
[27] L. Ke, B.N. Harmon, M.J. Kramer, *Electronic structure and magnetic properties in T_2AlB_2 (T = Fe, Mn, Cr, Co, and Ni) and their alloys*, Phys. Rev. B 95 (2017) 104427.
[28] R. Kieffer, F. Benesovsky, Hartstoffe, Springer Verlag, Wien, 1963.
[29] L.E. Toth, Transition Metal Carbides and Nitrides, Academic Press, New York, 1971.
[30] V.I. Matkovich, G.V. Samsonov, P. Hagenmuller, T. Lundstrom, Boron and Refractory Borides, Springer Verlag, Berlin, 1977.
[31] J.B. Levine, J.B. Betts, J.D. Garrett, S.Q. Guo, J.T. Eng, A. Migliori, R.B. Kaner, Full elastic tensor of a crystal of the superhard compound ReB2, Acta Mater. 58 (2010) 1530—1535.
[32] A.T. Lech, C.L. Turner, J. Lei, R. Mohammadi, S.H. Tolbert, R. B Kaner, Superhard rhenium/tungsten diboride solid solutions, J. Am. Chem. Soc. 138 (2016) 14398—14408.
[33] E. Deligoz, K. Colakoglu, Y.O. Ciftci, *Lattice dynamical and thermodynamical properties of ReB_2, RuB_2, and OsB_2 compounds in the ReB_2 structure*, Chin. Phys. B 21 (2012) 106301.
[34] P.E. Blochl, Projector augmented-wave method, Phys. Rev. B 50 (1994) 17953—17979.
[35] W. Kohn, L.J. Sham, Self-consistent equations including exchange and correlation effects, Phys. Rev. 140 (1965) A1133—A1138.
[36] P. Hohenberg, W. Kohn, Inhomogeneous electron gas, Phys. Rev. 136 (1964) B864—B871.
[37] G. Kresse, J. Furthmuller, Efficiency of ab initio total energy calculations for metals and semiconductors using a plane-wave basis set, Comput. Mater. Sci. 6 (1996) 15—50.
[38] J.P. Perdew, K. Burke, M. Ernzerhof, Generalized gradient approximation made simple, Phys. Rev. Lett. 77 (1996) 3865—3868.
[39] H.J. Monkhorst, J.D. Pack, Special points for Brillouin-zone integrations, Phys. Rev. B 13 (1976) 5188—5192.
[40] Y.L. Page, P. Saxe, Symmetry-general least-squares extraction of elastic coefficients from ab initio total energy calculations, Phys. Rev. B 63 (2001) 174103.
[41] R. Galliac, P. Pullumbi, F.-X. Coudert, ELATE: an open-source online application for analysis and visualization of elastic tensors, J. Phys. Condens. Matter 28 (2016) 275201—275205.
[42] J.W. Jaeken, S. Cottenier, Solving the Christoffel equation: phase and group velocities, Comput. Phys. Commun. 207 (2016) 445—451.
[43] A. Togo, I. Tanaka, First principles phonon calculations in materials science, Scripta Mater. 108 (2015) 1—5.
[44] K. Momma, F.J. Izumi, VESTA: a three-dimensional visualization system for electronic and structural analysis, Appl. Crystallogr. 41 (2008) 653—658.
[45] R.W.G. Wyckoff, Crystal Structures, vol. 1, John Wiley & Sons Ltd., 1963.
[46] G. Surucu, A. Gencer, X. Wang, O. Surucu, *Lattice dynamical and thermo-elastic properties of M_2AlB (M = V, Nb, Ta) MAX phase borides*, J. Alloys Compd. 819 (2020) 15325610.

[47] P. Vinet, J.H. Rose, J. Ferrante, J.R. Smith, Universal features of the equation of state of solids, J. Phys. Condens. Matter 1 (1989) 1941.
[48] J. Kudrnovsky, I. Turek, V. Drchal, F. Maca, P. Weinberger, P. Bruno, Exchange interactions in III-V and group-IV diluted magnetic semiconductors, Phys. Rev. B 69 (2004) 115208.
[49] A. Erkisi, G. Surucu, The investigation of electronic, magnetic, mechanical, and lattice dynamical properties of PdMX (M = Cr, Fe and X = Si and Ge) ferromagnetic half-Heusler metallics: an ab initio study, Mater. Res. Express 4 (2017), 066504.
[50] T. Yang, Z. Cheng, G. Surucu, X. Wang, *Coexistence of parabolic and linear band crossings and electron-doped spin-gapless properties in rhombohedral type $YbBO_3$*, J. Alloys Compd. 823 (2020) 153835.
[51] Y.L. Page, P. Saxe, Symmetry-general least-squares extraction of elastic coefficients from ab initio total energy calculations, Phys. Rev. B 63 (2001) 174103.
[52] C. Li, B. Wang, R. Wang, H. Wang, X. Lu, First-principles study of structural, elastic, electronic, and optical properties of orthorhombic BiGaO3, Comput. Mater. Sci. 42 (2008) 614–618.
[53] M.B. Baysal, G. Surucu, E. Deligoz, H. Ozısık, *The effect of hydrogen on the electronic, mechanical and phonon properties of $LaMgNi_4$ and its hydrides for hydrogen storage applications*, Int. J. Hydrogen Energy 43 (2018) 23397–23408.
[54] W. Voigt, B.G. Teubner, Lehrbuch der Kristallphysik [The textbook of crystal physics], 1928. Leipzig und Berlin.
[55] A. Reuss, Berechnung der Fliessgrenze von Mischkristallen auf Grund der Plastizitatsbedingung Fur Einkristalle [Calculation of the liquid limit of mixed crystals on the basis of the plasticity condition for single crystals], J. Appl. Math. Mech. 9 (1929) 49–58.
[56] R. Hill, The elastic behaviour of a crystalline aggregate, Proc. Phys. Soc. 65 (1952) 349–354.
[57] A. Erkisi, G. Surucu, *The electronic and elasticity properties of new half-metallic chalcogenides Cu_3TMCh_4 (TM = Cr, Fe and Ch = S, Se, Te): an ab initio study*, Philos. Mag. A 99 (2019) 513–529.
[58] V.V. Bannikov, I.R. Shein, A.L. Ivanovskii, *Electronic structure, chemical bonding and elastic properties of the first thorium-containing nitride perovskite $TaThN_3$*, Phys. Status Solidi 1 (2007) 89–91.
[59] S.F. Pugh, XCII. Relations between the elastic moduli and the plastic properties of polycrystalline pure metals, Lond. Edinb. Dubl. Phil. Mag. 45 (1954) 823–843.
[60] A.O. Lyakhov, A.R. Oganov, Evolutionary search for superhard materials: Methodology and applications to forms of carbon and TiO2, Phys. Rev. B 84 (2011), 092103, 092107.
[61] D. Pettifor, Theoretical predictions of structure and related properties of intermetallics, Mater. Sci. Technol. 8 (1992) 345–349.
[62] P. Ravindran, L. Fast, P.A. Korzhavyi, B. Johansson, J. Wills, O. Eriksson, *Density functional theory for calculation of elastic properties of orthorhombic crystals: Application to $TiSi_2$*, J. Appl. Phys. 84 (1998) 4891–4904.
[63] D.H. Chung, W.R. Buessem, The elastic anisotropy of crystals, J. Appl. Phys. 38 (1967) 2010–2012.
[64] S.I. Ranganathan, M. Ostoja-Starzewski, Universal elastic anisotropy index, Phys. Rev. Lett. 101 (2008), 055504.
[65] A. Gencer, G. Surucu, Investigation of structural, electronic and lattice dynamical properties of XNiH3 (X = Li, Na and K) perovskite type hydrides and their hydrogen storage applications, Int. J. Hydrogen Energy 44 (2019) 15173–15182.
[66] D.G. Cahill, S.K. Watson, R.O. Pohl, Lower limit to the thermal conductivity of disordered crystals, Phys. Rev. B 46 (1992) 6131–6140.
[67] D.R. Clarke, C.G. Levi, Materials design for the next generation thermal barrier coatings, Annu. Rev. Mater. Res. 33 (2003) 383–417.
[68] A.A. Maradudin, E.W. Montroll, G.H. Weiss, I.P. Ipatova, Theory of Lattice Dynamics in the Harmonic Approximation, Academic Press, New York, 1971.